

Cite this: *RSC Adv.*, 2018, 8, 31311

Environmentally sustainable route to SiO₂@Au–Ag nanocomposites for biomedical and catalytic applications†

Kanti Sapkota,^{ab} Prerna Chaudhary^{ab} and Sung Soo Han^{ab} 

A facile, sustainable, operationally simple and mild method for the synthesis of SiO₂@Au–Ag nanocomposites (NCs) using *Nephrolepis cordifolia* tuber extract is described and its catalytic, antibacterial and cytotoxic properties were investigated. The fabricated SiO₂@Au–Ag NCs were well characterized by UV-visible spectroscopy, transmission electron microscopy (TEM), energy-dispersive X-ray (EDX), Fourier transform infrared (FT-IR) spectroscopy, powder X-ray diffraction (XRD), thermogravimetric analysis (TGA) and X-ray photoelectron spectroscopy (XPS) to determine the optical activity, size and morphology, elemental composition, functional groups present, crystallinity, thermal stability and chemical state respectively. The obtained SiO₂@Au–Ag NCs exhibited spherical shape SiO₂ decorated with Au and Ag nanoparticles. The diameter of the SiO₂ nanoparticles ranges from 200–246 with average 3 nm diameter of Au and Ag NPs. Synthetic utility of this protocol has been demonstrated by exploring its effective catalytic activities for the solvent-free amidation of carboxylic acid with a primary amine with excellent yields. Moreover, the synthesized nanocomposite exhibited as noticeable antibacterial effect against Gram negative and Gram positive bacteria and better bio-compatibility against human keratinocytes. Thus, additive free SiO₂@Au–Ag NCs display the potential for catalysis and biomedical applications.

Received 26th May 2018
Accepted 30th August 2018
DOI: 10.1039/c8ra04502j
rsc.li/rsc-advances

Introduction

Recent advances in the synthesis of novel nanostructures with metal nanoparticles (Ag, Au, Fe, Cu, Ru, Pd, etc.) deposited on metallic oxide surfaces have gained substantial interest in nanotechnology and material science because of their significant applications in diverse fields such as biomedical, catalysis, bio-sensing, information storage, solar cells, optical and many more.^{1–7} Particularly important are silica-metal nanocomposites because of their broad applications in catalysis and biomedical fields.^{8,9} For example, silica based nanocomposites like SiO₂–Au, SiO₂–Ag and SiO₂–Au/Ag display noteworthy advantages in various fields of nanomedicine such as bioimaging, photothermal therapy, drug delivery, biosensing and catalysis due to their highly attractive properties such as tunable porous structure, remarkable plasmonic properties, unique composition, biocompatibility and physiochemical properties.^{10–12} Therefore, the silica-metal nanostructure is a widely used material due to its unique properties like optical transparency, porous structure, ability to functionalize pore

system, easy surface modification, biocompatibility and chemical stability.^{13–17} In addition, nanostructured Au and Ag materials are highly applicable in interfacial science and (bio)analytical chemistry because their optical properties are appropriate for applications of surface-sensitive techniques like surface enhanced Raman (SER) spectroscopy.^{18–25} Moreover, over the past few years, silver and gold nanoparticles have been increasingly used due to their powerful optical, electrical and microbial properties in various areas of research as biological sensors, catalysis, drug delivery vehicles, and anti-microbial agents as well as having low cytotoxic effects on mammalian cells.^{26–31}

Due to the wide applications and usefulness in various fields, silica-metal nanocomposites have been synthesized by various research groups. For example, β -cyclodextrin (β -CD) coated SiO₂@Au@Ag nanoparticles has been synthesized in a single-step reaction using β -CD as both the reducing and stabilizing agents for the surface-enhanced Raman scattering (SERS) detection of polychlorinated biphenyls (PCBs).³² Recently, silica coated Au/Ag nanomaterials have been reported for photothermal and photodynamic cancer therapy.³³ Moreover, Au, Ag, Pd/SiO₂ mesoporous nanocomposites has been synthesized by sonochemical approach.³⁴ Monodisperse α -Fe₂O₃@SiO₂@Au core/shell nanocomposite spheres has been synthesized by sol-gel process based on the modified Stöber method.³⁵ Gold/silver bi-metal nanodots on silica spheres prepared by *N*-[3-(trimethoxysilyl)propyl]diethylenetriamine and modified strobe method respectively and exhibited antimicrobial properties.³⁶

^aSchool of Chemical Engineering, Yeungnam University, 280 Daehak-Ro, Gyeongsan, Gyeongbuk 38541, Republic of Korea

^bDepartment of Nano, Medical & Polymer Materials, College of Engineering, Yeungnam University, 280 Daehak-Ro, Gyeongsan, Gyeongbuk 38541, Republic of Korea. E-mail: sshan@yu.ac.kr; Fax: +82-53-810-4686; Tel: +82-53-810-2773

† Electronic supplementary information (ESI) available: ¹H NMR and ¹³C NMR of the synthesized compounds. See DOI: 10.1039/c8ra04502j

In addition, highly sensitive surface-enhanced Raman scattering (SERS) probes based on $\text{SiO}_2\text{@Au@Ag}$ nanoparticles (NPs) and bifunctional $\text{Ag@SiO}_2/\text{Au}$ NPs for probing sequential catalytic reactions have been recently reported.^{37,38}

Though there are several reports for the synthesis of SiO_2 -metal nanomaterials, most of the reported methods utilize chemical approaches for the synthesis of such nanoparticles. However, these chemical based methods are toxic, hazardous and have side effects for health and environment. Moreover, using toxic and harmful chemicals for the fabrication of metal nanoparticles raises the environmental pollution and toxicity levels. Therefore development of environmental friendly, clean and green approach is necessary for the synthesis of metal nanoparticles to minimize the environmental impact and hazardous chemicals.^{39–42} In order to fulfill the need for developing environmentally benign methods, plant materials can be used as green material that can be easily available at low cost, easy to handle, renewable and more importantly non-toxic and environmental friendly for the preparation of number of metal and metal oxide nanoparticles.^{43–46} Very recently, we have reported Au-Ag@AgCl nanocomposites using AgNO_3 and HAuCl_4 precursor and the tuber extract of *Nephrolepis cordifolia* as a reducing and stabilizing agents.⁴⁷

As a continuous effort in developing environmentally benign method for the synthesis of metal nanomaterials, herein, we disclose the synthesis of $\text{SiO}_2\text{@Au-Ag}$ nanocomposites through a facile and green technique using tuber extract of *Nephrolepis cordifolia* which acts as both reducing and capping agents without using external additives (Scheme 1). Then, synthesized $\text{SiO}_2\text{@Au-Ag}$ NCs were checked for its catalytic potential for the solvent-free amidation of carboxylic acid with primary amine. Furthermore, antibacterial and cytotoxic activities were investigated using the synthesized $\text{SiO}_2\text{@Au-Ag}$ NCs.

Experimental

Materials and methods

Tetraethyl orthosilicate (TEOS; purity 99.9%), silver nitrate (AgNO_3 , 99%), gold(III) chloride trihydrate ($\text{HAuCl}_4 \cdot 3\text{H}_2\text{O}$, 99.9%)

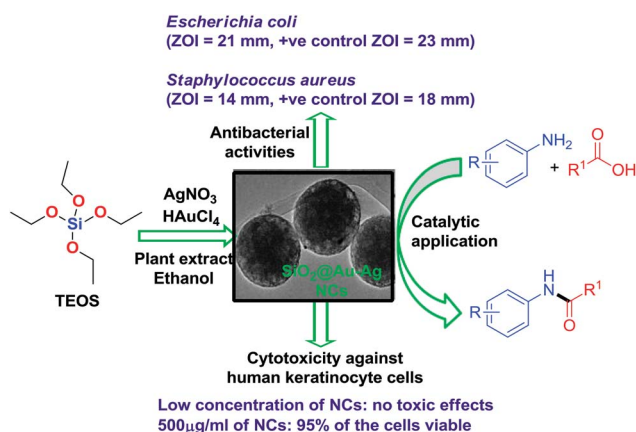
and ammonium hydroxide (NH_4OH) were purchased from Sigma-Aldrich. The fresh tubers of *Nephrolepis cordifolia* (L.) C. Presl was obtained from Kaski district of Nepal. Human keratinocyte cells [CCD 1102 KERTr (ATCC/CRL-2310)] were obtained from the American Type Culture Collection (ATCC). Dulbecco's medium, Phosphate Buffered Saline (PBS), fetal bovine serum (FBS), dimethyl sulphoxide (DMSO) was purchased from Sigma-Aldrich (St Louis, MO, USA). Penicillin, streptomycin, trypsin/EDTA and (4,5-dimethylthiazol-2-yl)-2,5-diphenyltetrazolium bromide (MTT) were also procured from Sigma-Aldrich. The bacterial strains of *Staphylococcus aureus*, (KCTC-1916) and *Escherichia coli* (KCTC-1924) were obtained from Korean Collection for Type Cultures (KCTC). Muller-Hinton broth media for bacterial culture and agar were procured from Becton, Dickinson and Company (Sparks, MD 21152 USA). Firstly, the used glassware was washed and rinsed with double distilled water and then dried in an oven. Double distilled water was used throughout the experiments. All the obtained chemicals were used as received without further purification. The tubers of *Nephrolepis cordifolia* was washed with double distilled water and dried at room temperature. The 5 grams of tubers were cut into small pieces and 100 mL of distilled water was added. Then, the mixture was boiled for 10 minutes. The resultant solution was centrifuged at 4000 rpm for 10 minutes and filtered.

Synthesis of SiO_2 NPs

Firstly 100 mL of prepared tuber extract of *Nephrolepis cordifolia* was mixed to 100 mL of ethanol in a 500 mL round bottom flask. Then the mixture was stirred using a magnetic bar for 30 min at 30 °C. After 30 min, 6 mL of tetraethyl orthosilicate (TEOS) added to the extract quickly by dropwise and the pH was adjusted 12.0 using ammonium hydroxide. The resultant mixture was vigorously stirred using a magnetic bar for 18 h and refluxed for 3 h. The presence of white precipitate indicated the formation of silica nanoparticles. Then the reaction was stopped and washed the solution with ethanol 4 times by centrifugation at 10 000 rpm, at 4 °C for 20 min (using a Labo-Gene 1580R centrifuge: Gyrozen). Finally SiO_2 nanoparticles was dried in a vacuum oven at 60 °C for 3 h and collected in a sterile airtight vial.

Synthesis of $\text{SiO}_2\text{@Au-Ag}$ nanocomposites (NCs)

The prepared 100 mg of SiO_2 nanoparticles (NPs) were dispersed in 100 mL double distilled water and sonicated for 1 h. Then, 10 mL of freshly prepared *Nephrolepis cordifolia* tuber extract solution was mixed with 100 mL of 2 mmol AgNO_3 aqueous solution and mixed with dispersed SiO_2 NPs solution and sonicated for 30 min. Subsequently, 100 mL of aqueous solution of 2 mmol HAuCl_4 and 10 mL of tuber extract was added to the dispersed solution. The resultant mixture of solutions was sonicated for 1 h. Then the brownish red color solution indicated the formation of $\text{SiO}_2\text{@Au-Ag}$ nanocomposites (NCs). The prepared NCs were washed and isolated by centrifugation at 10 000 rpm, at 4 °C for 20 min and the process was repeated four times and dried in a vacuum oven at 60 °C for 5 h.



Scheme 1 Green synthesis of recyclable $\text{SiO}_2\text{@Au-Ag}$ NCs and their diverse catalytic and biomedical applications.



Characterization of NCs

The surface plasmon resonance was performed in order to identify the formation of nanocomposites using a quartz cuvette by a UV-vis spectrophotometer (Shimadzu UV-2600). The powder X-ray diffraction (XRD) was recorded to confirm the crystallinity of the SiO₂@Au-Ag NCs using a PANalytical X'Pert PRO MPD unit operating at voltage 40 kV and 30 mA with Cu K α as the X-ray source ($\lambda = 1.5406 \text{ \AA}$) with scanning 2θ angle range, 20–90°, at rate of 1.2° min^{−1}. Fourier transform infrared (FT-IR) spectra were recorded using a Perkin-Elmer FT-IR spectrometer in transmittance mode between the wavenumber range 400–4000 cm^{−1}. For transmission electron microscopy (FE-TEM) sample was prepared by dipping the copper grid twice into the diluted and 2 h sonicated homogenised NCs sample solution. Then air dried grid was analysed to identify the size and shape of the synthesized NCs using field emission transmission electron microscopy (FE-TEM, FEI Tecnai F20). Similarly, the morphology of the synthesized NCs was characterized by field emission scanning electron microscopy (Fe-SEM, S4800, Hitachi, Ltd.) with an acceleration voltage of 5.0 kV. The elemental analysis of prepared NCs was performed using high-angle annular dark-field scanning TEM energy-dispersive X-ray spectroscopy (HAADF-STEM-EDS) at an accelerating voltage of 200 kV with a point resolution of 0.24 nm, a Cs and Cc of 1.2 mm each with a focal length of 1.7 mm, and by a Genesis liquid nitrogen cooled EDS detector.

X-ray photoelectron spectroscopy (XPS) was carried out to determine the surface chemistry and electronic states of prepared NCs using a Thermo Scientific K-Alpha system an Al K-alpha X-ray source with an ion source energy region of 100 V to 3 keV. Zeta potential of NCs was recorded using Zetasizer Nano ZS (Malvern Instrument). The sample was prepared in distilled water and sonicated for 30 min. The prepared sample was equilibrated for 2 min in a disposable cell and the measurement was conducted three times at 25 °C. Thermogravimetric analyses (TGA) was carried out by observing the percentage of mass loss using a differential scanning calorimeter (TG-DTA, SDT-Q600 V20.5 Build 15) in the temperature range 30 to 800 °C at a heating rate of 10 °C min^{−1} in N₂ atmosphere.

Catalytic activity

The synthesized SiO₂@Au-Ag NCs were used as excellent catalyst for the solvent-free amidation of carboxylic acid with primary amine.

General procedure for the solvent-free syntheses of amide derivatives 3a–3d

2 mol% SiO₂@Au-Ag NCs were added to a stirred solution of amine **1** (1.0 mmol) and carboxylic acid **2** (5.0 mmol). The reaction mixture was heated at 100 °C for 8 h and the progress of the reaction was monitored by TLC. After reaction completion, SiO₂@Au-Ag NCs were recovered *via* hot filtration as residue and the filtrate was subjected to silica gel column chromatography to isolate the pure products **3a–3d**.

Antibacterial activity of SiO₂@Au-Ag NCs

The antibacterial activities of the green synthesized nanocomposites were evaluated against Gram-positive (*S. aureus* KCTC-1916) as well as Gram-negative (*E. coli* KCTC-1924) bacterium using a modified disc diffusion method.⁴⁸ Briefly, 3–4 colonies of each bacterium were inoculated in 10 mL of Mueller–Hinton (M–H) broth medium and the bacteria were grown at 37 °C in a shaking incubator at 200 rpm until the optical density (O.D) was reached 0.8 at 600 nm. From this bacterial suspension, 100 μ L was spread over M–H agar plates. Various concentrations of nanoparticles (50–200 μ g mL^{−1}) were added to the sterilized 6 mm filter discs (Whatman, GE Healthcare UK Limited) placed on the M–H agar plates. Ampicillin (200 mg L^{−1}) was used as reference positive control for the experiments. All the plates were incubated at 37 °C for 24 h and the diameters of zone of inhibition were measured. All the experiments were performed in triplicates and mean diameter was calculated.

In vitro cytotoxicity assay

The cytotoxic effect of SiO₂, SiO₂@Au, SiO₂@Ag and SiO₂@Au-Ag nanocomposites was analyzed using a standard MTT (3-(4,5-dimethylthiazol-2-yl)-2,5-diphenyltetrazolium bromide) assay. Human keratinocyte cells were used to assess the cytotoxic effects of the nanoparticles. Briefly, keratinocyte cells [CCD 1102 KERTr (ATCC/CRL-2310)] were grown in Dulbecco's modified Eagle's (DMEM) medium supplemented with 10% fetal bovine serum along with 100 U mL^{−1} penicillin–streptomycin in a humidified environment containing 5% CO₂/95% air at 37 °C. After reaching the confluence, cells were passaged and seeded in a 96 well plate at a density of 1 \times 10⁵ cells per well for overnight. Next day, the cells were treated with various concentrations (50–500 μ g mL^{−1}) of nanoparticles in triplicates and kept for 24–96 h at 37 °C in a humidified environment. Untreated cells were used as a control.

After treatment, old media was removed and each well was washed with PBS followed by incubation with 50 μ L of MTT (5 mg mL^{−1} stock) for 4 h. The purple colored formazan crystal formed, were dissolved in 200 μ L DMSO. The absorbance was taken at 570 nm using a multi well ELISA plate reader (BioTek Instruments, Inc., USA). The cell viability were measured using the formula-

$$\text{Cell viability} = (\text{O.D of experiment} / \text{O.D. of control}) \times 100$$

All the readings were taken in triplicates and a graph showing percentage cell viability was plotted against nanoparticles concentration.

Results and discussion

Characterization of SiO₂@Au-Ag NCs

Firstly, formation of brownish red color resultant solution indicated the formation of SiO₂@Au-Ag nanocomposites. Fig. 1 illustrates the UV spectra of SiO₂, SiO₂@Ag, SiO₂@Au and



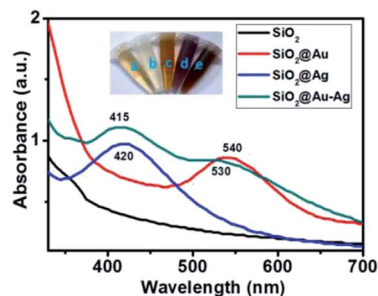


Fig. 1 UV-vis spectra of SiO_2 , $\text{SiO}_2\text{@Ag}$, $\text{SiO}_2\text{@Au}$ and $\text{SiO}_2\text{@Au-Ag}$. The inset images show: (a) plant extract, (b) SiO_2 , (c) $\text{SiO}_2\text{@Ag}$, (d) $\text{SiO}_2\text{@Au}$ and (e) $\text{SiO}_2\text{@Au-Ag}$ NCs.

$\text{SiO}_2\text{@Au-Ag}$ nanocomposites. The prepared $\text{SiO}_2\text{@Au-Ag}$ nanocomposites showed the characteristic surface plasmon resonance (SPR) bands at 415 nm and 530 nm which can be attributed to the SPR of Au-Ag formed on the surface of SiO_2 where $\text{SiO}_2\text{@Au}$ NCs was observed at 540 nm. The strong absorption band of $\text{SiO}_2\text{@Ag}$ NCs was observed at 420 nm which ascribed to the formation of Ag on the surface of SiO_2 . The observed characteristic SPR peaks and color change of the NCs indicated the formation of $\text{SiO}_2\text{@Au-Ag}$ nanocomposites.

Fig. 2 shows the powder X-ray diffraction pattern of $\text{SiO}_2\text{@Au-Ag}$ synthesized from *Nephrolepis cordifolia* with intense characteristic peaks. In Fig. 2, the XRD peaks of *Nephrolepis cordifolia* mediated $\text{SiO}_2\text{@Au-Ag}$ observed at 2θ value of 38.2° , 44.4° , 64.6° , 77.6° and 81.7° were indexed to the reflection planes (111), (200), (220), (311), and (222) respectively, due to the face-centred cubic phase of silver (JCPDS no. 04-0784) and cubic gold (JCPDS no. 04-0783), which confirmed the crystalline nature of Ag and Au metal species, whereas SiO_2 NPs didn't show any phase pattern because of amorphous in phase. The diffraction pattern of the silica nanoparticles were studied around 21° at 2θ value.

Fig. 3a shows the FT-IR spectra of synthesized nanocomposites which analyze functional groups present in the *Nephrolepis cordifolia* mediated $\text{SiO}_2\text{@Au-Ag}$ NCs as both capping agents as well as reducing agents which are responsible for the fabrication of nanocomposites. As presented in Fig. 3a, the absorption band at 3219 cm^{-1} of obtained $\text{SiO}_2\text{@Au-Ag}$ NCs

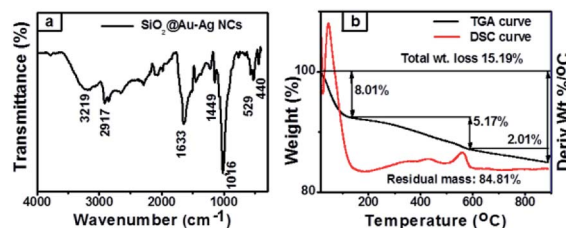


Fig. 3 (a) FT-IR spectra and (b) TGA and DSC curve of $\text{SiO}_2\text{@Au-Ag}$ NCs.

corresponds to O-H stretching of alcohols or phenols and aromatic C-H stretching. The absorption peaks at wave number 1633 cm^{-1} assigned to asymmetric stretching of COO^- and 1449 cm^{-1} are attributed to the symmetric stretching. The FTIR absorption band observed at around 1016 cm^{-1} corresponds to asymmetric vibration of Si-O-Si.⁴⁹

A number of bioactive molecules present in the plant materials play a vital role as a reducing and capping agents for the formation of nanocomposites. The reducing phytochemicals which bind and capped the metal ion to form the stable nanoparticles as mechanism presented in Fig. 4. Therefore, the organic molecules which played the main role for formation of $\text{SiO}_2\text{@Au-Ag}$ nanocomposites are phytol, ethyl palmitate, β -ionone, ethyl linolenate diterpene alcohol, eugenol, anethol and α -cadinol which have been extracted from *Nephrolepis cordifolia*.⁵⁰

Thermal stability of $\text{SiO}_2\text{@Au-Ag}$ NCs prepared from tuber extract of *Nephrolepis cordifolia* was examined by DSC-TGA as illustrated in Fig. 3b. The sample of prepared NCs was subjected at temperature starting from room temperature to 900°C with ramp rate $10^\circ\text{C min}^{-1}$ under nitrogen atmosphere. The decomposition of mass was recorded in three successive steps. The first step of mass loss was found to be 8.01% around temperature 100°C due to the moisture and some volatile compounds contains in the sample. Secondly, 5.17% and finally 2.1% mass loss at the decomposition temperature 430°C and

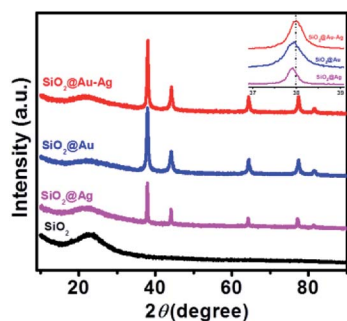


Fig. 2 XRD patterns of the SiO_2 , $\text{SiO}_2\text{@Ag}$, $\text{SiO}_2\text{@Au}$ and $\text{SiO}_2\text{@Au-Ag}$ NCs. Inset shows the magnified view of $\text{SiO}_2\text{@Au-Ag}$, $\text{SiO}_2\text{@Au}$ and $\text{SiO}_2\text{@Ag}$.

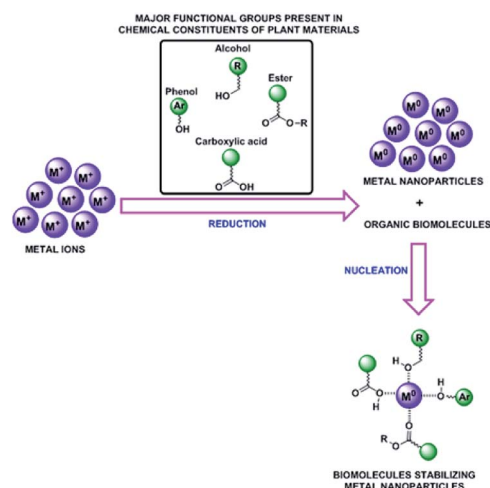


Fig. 4 Proposed mechanisms for the green synthesis of $\text{SiO}_2\text{@Au-Ag}$ NCs.



beyond 900 °C were examined respectively due to the loss of capping agents and other bioactive molecule present on the *Nephrolepis cordifolia* mediated NCs. Thus, the total percentage of mass degradation (15.19%) was observed in TGA graph. The remaining percentage of mass (84.81%) of sample indicated the existence of Si, O, Au and Ag in biosynthesized $\text{SiO}_2\text{@Au-Ag}$ NCs.

TEM and SEM analysis revealed the morphology and size of the $\text{SiO}_2\text{@Au-Ag}$ NCs prepared from *Nephrolepis cordifolia* tuber (Fig. 5). Fig. 5a–f displays TEM images and HR-TEM of $\text{SiO}_2\text{@Au-Ag}$ NCs which confirmed the spherical shape of Au and Ag nanoparticles decorated on the porous spherical shape silica nanoparticles. TEM micrographs investigated the poly-dispersed silica nanoparticles with size ranges 200–246 nm. HRTEM image clearly showed the well dispersed silver–gold nano particles on the porous silica nanoparticles (Fig. 5b–f). Similarly, SEM analysis displayed the spherical morphology of the synthesized NCs and the Au and Ag NPs could not be clearly visible on the surface of SiO_2 due to the very small size of Au and Ag NPs (3 nm) in low resolution SEM (Fig. 5g–i). The formation of $\text{SiO}_2\text{@Au-Ag}$ system could be due to the strong interaction of Au–Ag metals with the support material SiO_2 . In general, SiO_2 is regarded as an inert support and does not show significant metal support interaction (SMSI). However, in Pt– SiO_2 system, SMSI effect has been demonstrated.⁵¹ Moreover, a covalent interaction has been reported between metal atoms and surface anions in metal– SiO_2 system.^{52,53} Fig. 6a–e display HAADF-STEM images of Si, O, Au and Ag present in the $\text{SiO}_2\text{@Au-Ag}$ NCs using the high-angle annular dark-field imaging with scanning transmission electron microscopy (HAADF-STEM). Fig. 6f shows the SAED pattern of the $\text{SiO}_2\text{@Au-Ag}$ NCs. Furthermore, energy-dispersive X-ray spectroscopy (EDS) analysis revealed the elemental composition of synthesized nanocomposites which confirmed the presence of Si, O, Au and Ag element in the $\text{SiO}_2\text{@Au-Ag}$ NCs (Fig. 6g).

XPS survey spectra of synthesized nanocomposites which confirmed the chemical state of the NCs and further clarified

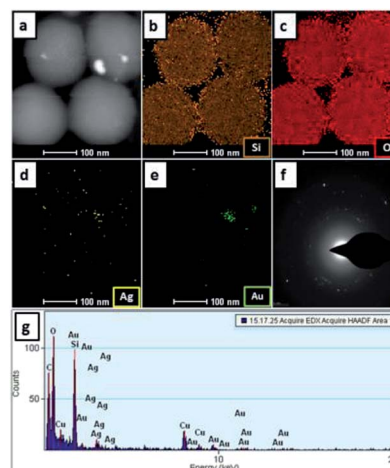


Fig. 6 HAADF-STEM micrographs at 100 nm (a–e), (f) SAED pattern and (g) EDS elemental mapping of Si, O, Au and Ag in $\text{SiO}_2\text{@Au-Ag}$ NCs.

the silica, gold and silver along with carbon elements present in the obtained $\text{SiO}_2\text{@Au-Ag}$ NCs (Fig. S1, ESI†). The spectrum of carbon element present in the figure indicated the presence organic compound in plant mediated $\text{SiO}_2\text{@Au-Ag}$ NCs. As presented in Fig. 7a, the single Si 2p spectrum at 103.5 eV attributed to the binding energy of Si in SiO_2 .³⁵ Similarly, the XPS Au 4f spectra displayed the double bands at 84.6 eV and 88.4 eV binding energies for Au 4f_{7/2} and Au 4f_{5/2} respectively in agreement with the characteristic binding energy of Au⁰ (Fig. 7c).⁵⁴ In Fig. 7d, Ag 4d XPS band showed two peaks at the binding energies of 368.8 eV and 374.8 eV which belong to Ag 3d_{5/2} and Ag 3d_{3/2} along with spin splitting of 6.0 eV respectively which confirmed the presence of Ag⁰.^{55,56} From the XPS analysis, the surface atomic percentage of Si, O, Au and Ag was found to be 30.07%, 68.49%, 0.22% and 1.21% respectively.

Stability analysis of $\text{SiO}_2\text{@Au-Ag}$

The stability of green synthesized $\text{SiO}_2\text{@Au-Ag}$ NCs using *Nephrolepis cordifolia* was evaluated as shown in Fig. 8. Firstly,

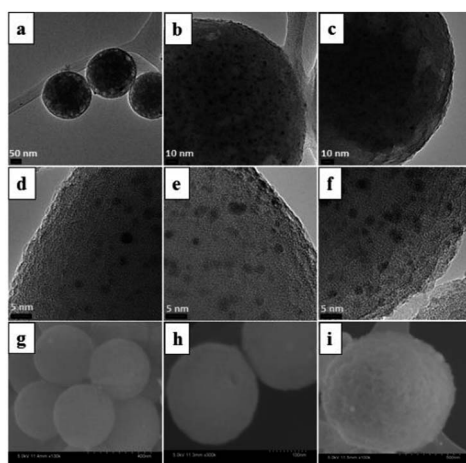


Fig. 5 TEM images of $\text{SiO}_2\text{@Au-Ag}$ NCs at scale bar (a) 50 nm, (b) 10 nm (c) 10 nm (d) 5 nm (e) 5 nm (f) 5 nm and SEM images at (g) 400 nm (h) 100 nm and (i) 500 nm.

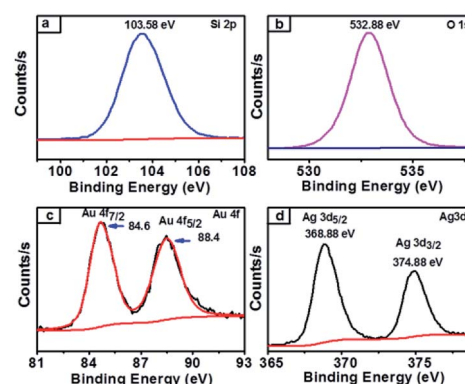


Fig. 7 XPS spectra of $\text{SiO}_2\text{@Au-Ag}$ NCs (a) Si 2p-electrons of silica containing NCs (b) O 1s-electrons of oxygen containing NCs (c) Au 4f-electrons of gold containing NCs and (d) Ag 3d-electrons of silver containing NCs.



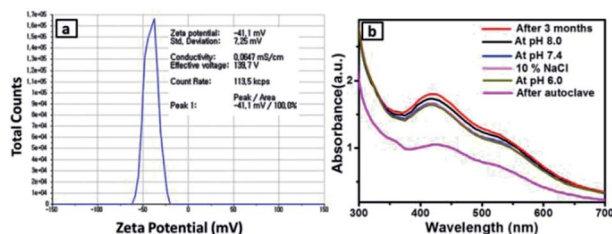


Fig. 8 (a) Zeta potential of the NCs. and (b) UV-vis spectra in various conditions (after 3 months, pH 6.0, pH 7.4, pH 8.0, 10% NaCl and after autoclave).

the prepared NCs was analysed by observing zeta potential distribution and the value was obtained 41.1 mV. The higher negative zeta potential value of *Nephrolepis cordifolia* stabilized $\text{SiO}_2\text{@Au-Ag}$ NCs confirmed the formation of stable NCs (Fig. 8a).^{47,57} Furthermore, the surface plasmon resonance (SPR) spectra of prepared $\text{SiO}_2\text{@Au-Ag}$ NCs was investigated using spectrophotometry in various conditions such as in different pH conditions (at pH 8, 7.4, and 6) along with using 10% NaCl and after autoclave the sample at 121 °C for 60 min. The Fig. 8b displays the SPR peaks which showed nearly same wave length (~425 nm) in every condition, which further confirmed the stability of green synthesized $\text{SiO}_2\text{@Au-Ag}$ NCs in biological fluids.

Catalytic activity

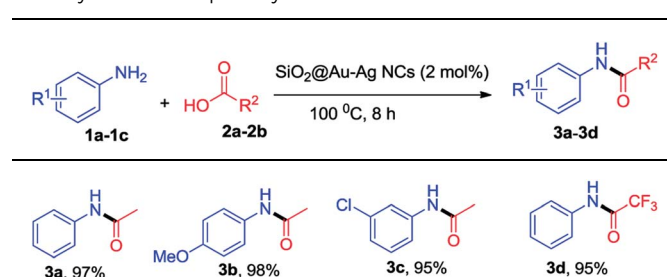
The optimization of reaction condition for the solvent free amidation of carboxylic acid is presented in Table 1. The highest yield of the product **3a** was obtained using $\text{SiO}_2\text{@Au-Ag}$ NCs compared to other catalysts such as SiO_2 , $\text{SiO}_2\text{@Ag}$, $\text{SiO}_2\text{@Au}$. In absence of catalyst, the yield was even lower. Based on the optimization study, catalytic activities of the synthesized $\text{SiO}_2\text{@Au-Ag}$ NCs for the solvent-free amidation of carboxylic acid with primary amine is summarized in Table 2. Reaction of aniline (**1a**) with acetic acid (**2a**) in the presence 2 mol% $\text{SiO}_2\text{@Au-Ag}$ NCs at 100 °C for 8 h provided amide **3a** in 97% yield (entry 1, Table 2). Similarly, reaction between 4-methoxy

Table 1 Optimization of the reaction conditions for the synthesis of **3a**^a

Entry	Catalyst (2 mol%)	Conditions	Yield ^b (%)
1	SiO_2	8 h, 100 °C	56
2	$\text{SiO}_2\text{@Ag}$	8 h, 100 °C	65
3	$\text{SiO}_2\text{@Au}$	8 h, 100 °C	67
4	$\text{SiO}_2\text{@Au-Ag}$	8 h, 100 °C	97
5	—	8 h, 100 °C	32

^a Reaction conditions: amine **1a** (1.0 mmol), carboxylic acid **2a** (5 mmol). ^b Isolated yield.

Table 2 $\text{SiO}_2\text{@Au-Ag}$ NCs catalyzed solvent free amidation of carboxylic acid with primary amine^a



^a Reaction conditions: amine **1** (1.0 mmol), carboxylic acid **2** (5 mmol) and $\text{SiO}_2\text{@Au-Ag}$ NCs (2.0 mol%).

aniline (**1b**) or 2-chloro aniline (**1c**) and aniline (**2a**) with acetic acid (**2a**) in the presence 2 mol% $\text{SiO}_2\text{@Au-Ag}$ NCs at 100 °C for 8 h provided the desired products **3b** and **3c** in 98% and 95% yields respectively (entry 2 and 3, Table 2). Moreover, treatment of aniline (**1a**) with trifluoroacetic acid (**2b**) in the presence 2 mol% $\text{SiO}_2\text{@Au-Ag}$ NCs at 100 °C for 8 h provided amide **3d** in 95% yield (entry 4, Table 2). These results demonstrate the efficient catalytic activities of the synthesized $\text{SiO}_2\text{@Au-Ag}$ NCs for the solvent-free amidation of carboxylic acid with primary amine in good yield. The structure of compounds **3a-3d** was identified by ¹H and ¹³C NMR and by direct comparison with reported data (data and spectra of the synthesized compounds are presented in the ESI†).

Comparative study of the $\text{SiO}_2\text{@Au-Ag}$ NCs with other catalysts

The enhanced catalytic performance of the synthesized $\text{SiO}_2\text{@Au-Ag}$ NCs can be evaluated by comparing the observed result with that of other reported catalysts. The results are outlined in Table 3.⁵⁸⁻⁶³ We compared the results of solvent free amidation of carboxylic acid with primary amine in the presence of various catalysts with respect to the solvent, temperature and product yield. Eventhough, the reported methods have their own advantages, the amidation of carboxylic acid in the presence of the biosynthesized $\text{SiO}_2\text{@Au-Ag}$ NCs were carried out rapidly with high yields and low loading of the catalyst.

Antimicrobial activity of $\text{SiO}_2\text{@Au-Ag}$ NCs

The antibacterial activity of synthesized nanoparticles was investigated against *Staphylococcus aureus* and *Escherichia coli* bacteria. The bactericidal effects of different nanoparticles as depicted by the zone of inhibition are shown in the Fig. 9. From the results, different patterns of zone of inhibition were observed. As shown in the figure, $\text{SiO}_2\text{@Au-Ag}$ nanocomposites were found to be most effective against both Gram-positive as well as Gram-negative bacterium at all the concentrations; on the other hand SiO_2 nanoparticles were inert for both bacterial species at all the tested particle concentrations (Fig. 9). $\text{SiO}_2\text{@Au}$ nanoparticles were also found to be inactive for Gram-positive bacterium at all the concentrations used, whereas for Gram-negative bacterium, only at higher concentration (200 µg



Table 3 Comparative catalytic activity of SiO₂@Au–Ag with other catalysts

Entry	Catalyst	Temperature	Yield (%)	Ref.
1	Thiamine hydrochloride	100 °C	90	58
2	PANI emeraldine	Dioxane, reflux	87	59
3	Nb ₂ O ₅	Toluene, reflux	80	60
4	rGO-SO ₃ H	Ultrasonic, rt	94	61
5	Yttria-zirconia	125 °C	93	62
6	Starbon-400-SO ₃ H	130 °C	87	63
7	SiO ₂ @Au–Ag NCs	100 °C	97	Present work

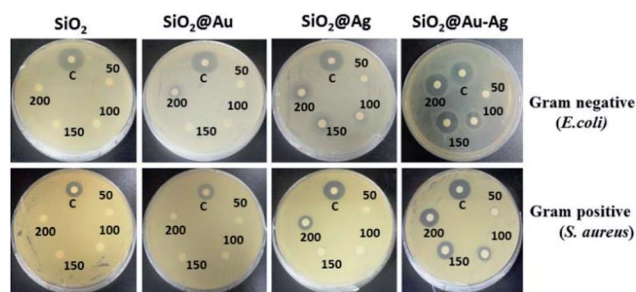


Fig. 9 Images of comparative antibacterial studies of different nanoparticles SiO₂, SiO₂@Au, SiO₂@Ag and SiO₂@Au–Ag at different concentration 50 µg mL^{−1}, 100 µg mL^{−1}, 150 µg mL^{−1}, 200 µg mL^{−1} against bacteria *E. coli* and *S. aureus* with respect to positive control of ampicillin (200 µg mL^{−1}).

mL^{−1}), an inhibition zone of 10 mm could be seen (Fig. 9). Although the exact mechanism of antibacterial effect of gold nanoparticles is not fully understood but it is assumed that Au NPs binds to the cell wall of the bacterium and suppressed bacterial growth at the first stage of their reproduction.⁶⁴ Due to their well-developed surface chemistry and the smaller size, gold nanoparticles can interact with the microorganisms with ease and cause destructive effects on them.⁶⁵

SiO₂@Ag nanoparticles showed better antibacterial effects than the SiO₂@Au nanoparticles and were able to hinder the growth of both bacterial species. This difference might be due to the strong antibacterial properties of silver. In case of SiO₂@Ag nanoparticles, the inhibition diameter for *E. coli* was measured 0, 7, 11 and 18 mm at a particle concentration of 50 µg mL^{−1}, 100 µg mL^{−1}, 150 µg mL^{−1} and 200 µg mL^{−1}

respectively, whereas for *S. aureus* it was measured 6.5 and 12 mm at 150 and 200 µg mL^{−1} concentrations respectively, Table 2 (Fig. 9). Silver nanoparticles bind to the thiol groups present on the bacterial membrane and create the pores on the cell membrane which leads to the death of the bacterium.⁶⁶ In case of SiO₂@Au–Ag nanoparticles, a clearance zone of 7, 13, 18 and 21 mm was measured against *E. coli* at 50 µg mL^{−1}, 100 µg mL^{−1}, 150 µg mL^{−1} and 200 µg mL^{−1} concentrations respectively as shown in Table 2. A diameter of 23 mm was measured for positive control ampicillin (200 µg mL^{−1}), which was comparable to the nanoparticles concentration. However, zone of inhibition of 7, 10, 13 and 14 mm was observed against Gram positive bacteria *S. aureus* at 50 µg mL^{−1}, 100 µg mL^{−1}, 150 µg mL^{−1} and 200 µg mL^{−1} concentrations respectively (Table 4 and Fig. 9).

The highest antibacterial activities displayed by SiO₂@Au–Ag nanocomposites might be due to the synergistic effect of Au–Ag nanoparticles. When particles are alone, they are likely to be aggregate and their surface gets oxidized, which in turn reduce their antibacterial performances, on the other hand together they tend to be more stable with higher antimicrobial activities.⁶⁷ The Gram-positive bacterium were less sensitive to the nanoparticles in comparison to the Gram-negative bacterium, and only a higher concentrations of nanoparticles could inhibit the growth of Gram-positive bacterium. This might be due to the presence of thick, lipoteichoic acid containing peptidoglycan cell wall around the Gram-positive bacterial membrane, which was difficult to cross by nanoparticles at lower concentrations.⁶⁸

Table 4 Antibacterial activity of *Nephrolepis cordifolia* mediated SiO₂, SiO₂@Au, SiO₂@Ag and SiO₂@Au–Ag NCs using disc diffusion method

Concentration (mg mL ^{−1})		Zone of inhibition (ZOI) in mm			
		SiO ₂	SiO ₂ @Au	SiO ₂ @Ag	SiO ₂ @Au–Ag
Gram –ve bacteria <i>E. coli</i> (KCTC-1924)	50	—	—	—	7
	100	—	—	—	13
	150	—	—	7	18
	200	—	10	11	21
Gram +ve bacteria <i>S. aureus</i> (KCTC-1916)	50	—	—	—	7
	100	—	—	—	10
	150	—	—	6.5	13
	200	—	—	12	14

For positive control ampicillin (200 mg mL^{−1}) ZOI = 23 mm

For positive control ampicillin (200 mg mL^{−1}) ZOI = 18 mm



Analysis of cytotoxic effects of nanocomposites

The cytotoxic effect of SiO_2 , $\text{SiO}_2\text{@Au}$, $\text{SiO}_2\text{@Ag}$ and $\text{SiO}_2\text{@Au-Ag}$ nanocomposites on human keratinocyte cells was studied using the MTT assay (Fig. 10). MTT assay helps in determination of cell viabilities *in vitro* conditions. The dehydrogenase enzymes present in the metabolically active cells convert yellow colored MTT (3-(4,5-dimethylthiazol-2-yl)-2,5-diphenyl tetrazolium bromide) salt solution to an insoluble violet-blue formazan which can be dissolved in organic solvents like DMSO and analyzed spectrophotometrically. The number of viable cells is directly proportional to the intensity of formazan crystal produced.⁶⁹ The viability of the cells depends on various factors like, concentration, shape, size and incubation period of the nanoparticles.⁷⁰ The results obtained showed concentration dependent cytotoxic effects on keratinocytes after exposure of the cells to the various concentrations ($50\text{--}500\text{ }\mu\text{g mL}^{-1}$) of nanoparticles. With the increase in the exposure time of nanoparticles from 24–96 hours, cytotoxicity was also increased. As shown in the Fig. 10, SiO_2 nanoparticles were most toxic to the cells, and in 96 hours at a concentration of $500\text{ }\mu\text{g mL}^{-1}$, almost 40% of the cells were dead. It is assumed that the SiO_2 nanoparticles interact with the macromolecules of the cells which activate the apoptotic and p53 pathway leading to the generation of reactive oxygen species (ROS) and finally causing the death of the cells.⁷¹ $\text{SiO}_2\text{@Ag}$ nanoparticles also induced cellular toxicity to the keratinocyte cells in a concentration and time dependent manner. After exposure of keratinocyte cells to $\text{SiO}_2\text{@Ag}$ nanoparticles at a concentration of $500\text{ }\mu\text{g mL}^{-1}$ for 96 hours, the cell viability was reduced to 75% (Fig. 10). It is supposed that $\text{SiO}_2\text{@Ag}$ nanoparticles bind to the cell membranes which disturb membrane permeability by increasing the ionic concentration and the oxidative stress causes the cell death.⁷² $\text{SiO}_2\text{@Au}$ nanoparticles were not very much toxic to the keratinocyte cell and longer exposure of the

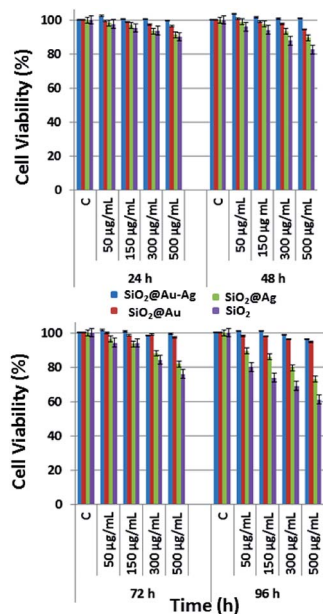


Fig. 10 Cytotoxic effect of different nanoparticles SiO_2 , $\text{SiO}_2\text{@Au}$, $\text{SiO}_2\text{@Ag}$ and $\text{SiO}_2\text{@Au-Ag}$ with different concentrations $50\text{ }\mu\text{g mL}^{-1}$, $150\text{ }\mu\text{g mL}^{-1}$, $300\text{ }\mu\text{g mL}^{-1}$ and $500\text{ }\mu\text{g mL}^{-1}$ on human keratinocytes.

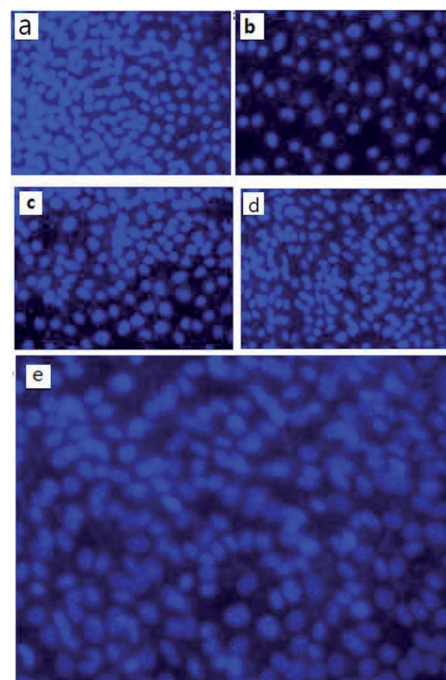


Fig. 11 Representative images from independent experiments when human keratinocyte cells were treated with biosynthesized nanoparticles at $500\text{ }\mu\text{g mL}^{-1}$ concentration and cells stained with DAPI after 96 hours, (a) control cells (b) cells treated with SiO_2 (c) $\text{SiO}_2\text{@Ag}$ (d) $\text{SiO}_2\text{@Au}$ and (e) $\text{SiO}_2\text{@Au-Ag}$ NCs.

cells with higher concentrations of nanoparticles could exert their cytotoxic effect (Fig. 10). Conceptually, the cellular uptake of nanoparticles increases with the increase in their concentration and treatment time, which cause higher cytotoxic effect on the cells.⁷³ Maximum viability, was observed in the cells which were treated with $\text{SiO}_2\text{@Au-Ag}$ nanocomposites. From Fig. 10, it can be seen that only the highest concentration $500\text{ }\mu\text{g mL}^{-1}$ of particle induced the cell death and at this concentration 95% of the cells were viable, however the lower concentrations of nanoparticles did not exert any toxic effect on the cells. The expected reason might be the tight binding of the gold and silver cations on to the surface of silica nanoparticles, which caused a slow release of Ag and Au ions causing higher cell viabilities.⁷⁴ These results demonstrate that the

Table 5 Recyclability of the $\text{SiO}_2\text{@Au-Ag}$ NCs^a

Entry	Cycle	Yield ^b (%)
1	First	97
2	Second	95
3	Third	93
4	Fourth	92
5	Fifth	90

^a Reaction conditions: amine **1a** (1.0 mmol), acid **2a** (5.0 mmol), $\text{SiO}_2\text{@Au-Ag}$ nanocatalyst (2 mol%). ^b Isolated yield.



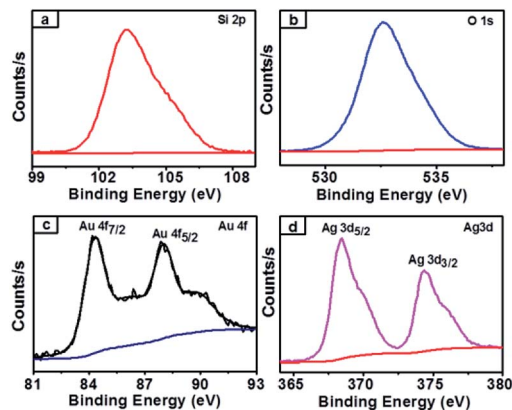


Fig. 12 XPS spectra of $\text{SiO}_2\text{@Au-Ag}$ NCs after recycle (a) Si 2p-electrons of silica (b) O 1s-electrons of oxygen (c) Au 4f-electrons of gold (d) Ag 3d-electrons of silver of $\text{SiO}_2\text{@Au-Ag}$ NCs.

synthesized nanocomposite is safe and biocompatible for potential bio-medical applications.

The cytotoxic effect of nanoparticles on human keratinocyte cells was further evaluated by staining with DAPI (4',6-diamidino-2-phenylindole). Briefly, 1×10^3 cells keratinocyte cells were seeded into culture plates and were incubated in a CO_2 incubator at 37°C for 24 hours. We can correlate these results with that of MTT assay, where similar kind of effects were observed. Both MTT and cell staining experiments showed a concentration dependent cell death of keratinocyte cells after treatment with the biosynthesized nanoparticles (Fig. 11).

Recyclability of catalyst

$\text{SiO}_2\text{@Au-Ag}$ NCs fabricated by *Nephrolepis cordifolia* was recycled and reprocessed five times without loss of any chemical compositions and catalytic activities (Table 5). After the completion of each reaction, the nanocatalyst was recovered by washing with ethyl acetate followed by hot water filtration for four times. Then the recycled nanocatalyst was dried in a vacuum oven for 4 h at 70°C . In order to investigate the stability of the recycled nanocatalysts, XRD and XPS analysis was further performed. The XPS and XRD results showed the similar surface chemical compositions and crystallinity of the synthesized $\text{SiO}_2\text{@Au-Ag}$ nanocomposites before and after catalysis process without any alterations (Fig. S1, ESI,[†] Fig. 12 and 13).

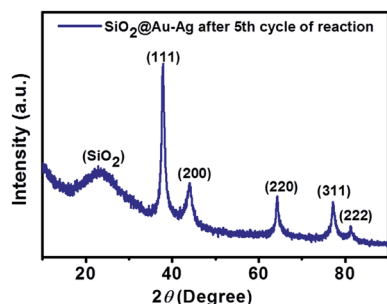


Fig. 13 XRD pattern of $\text{SiO}_2\text{@Au-Ag}$ NCs after fifth cycle of reaction.

Conclusions

An efficient, external additive-free and green approach for the facile synthesis of $\text{SiO}_2\text{@Au-Ag}$ NCs using tuber extract of *Nephrolepis cordifolia* was successfully developed. The morphology and size of the synthesized Au/Ag nanocomposites with an average diameter of 3 nm decorated in silica nanoparticles with highly dispersed manner were investigated by transmission electron microscopy (TEM) analysis. The crystallinity and functional group present in the plant mediated NCs were confirmed by X-ray diffraction (XRD) and Fourier transform infrared (FT-IR) analysis. Chemical composition and oxidation state of prepared NCs were confirmed by XPS and EDS analysis. Synthetic functions of fabricated nanocatalyst were established by solvent-free amidation of carboxylic acid with primary amine. In addition, the synthesized nanocomposites demonstrated efficient catalytic activity along with good recyclability. Furthermore, the prepared nanocomposites showed potent bactericidal activities and good biocompatibility. Therefore, the green synthesized $\text{SiO}_2\text{@Au-Ag}$ nanocomposites could be used as cost effective, sustainable, additive free, effective catalyst in organic synthesis as well as safe and biocompatible NCs for *in vivo* bio-medical applications.

Conflicts of interest

The authors declare no competing financial interest.

Acknowledgements

This research was fully supported from 2016 Yeungnam University Research Grant. The authors would like to acknowledge Basic Science Research Programme through the National Research Foundation of Korea (NRF) funded by the Ministry of Education, Science and Technology (NRF-2017R1D1A3B03031234).

References

- 1 T. Liu, D. Li, D. Yanga and M. Jiang, *Chem. Commun.*, 2011, 47, 5169.
- 2 Y. G. Sun and C. H. Lei, *Angew. Chem., Int. Ed.*, 2009, 48, 6824.
- 3 C. Wang, H. Daimon and S. H. Sun, *Nano Lett.*, 2009, 9, 1493.
- 4 F. Wang, G. M. Pauletti, J. Wang, J. Zhang, R. C. Ewing, Y. Wang and D. Shi, *Adv. Mater.*, 2013, 25, 3485.
- 5 L. Zhang, Y. Chen, Z. Li, L. Li, P. Saint-Cricq, C. Li, J. Lin, C. Wang, Z. Su and J. I. Zink, *Angew. Chem., Int. Ed.*, 2016, 55, 2118.
- 6 M. B. Gawande, A. Goswami, F.-X. Felpin, T. Asefa, X. Huang, R. Silva, X. Zou, R. Zboril and R. S. Varma, *Chem. Rev.*, 2016, 116, 3722.
- 7 S. Kumar, N. Harrison, R. K. Richards and K. Sokolov, *Nano Lett.*, 2007, 7, 1338.
- 8 Y. Tao, E. Ju, J. Ren and X. Qu, *Adv. Mater.*, 2015, 27, 1097.
- 9 J. V. Jokerst, M. Thangaraj, P. J. Kempen, R. Sinclair and S. S. Gambhir, *ACS Nano*, 2012, 7, 5920.



- 10 R. Liu, Y. Zhang, X. Zhao, A. Agarwal, L. J. Mueller and P. Feng, *J. Am. Chem. Soc.*, 2010, **132**, 1500.
- 11 I. I. Slowing, J. L. Vivero-Escoto, C. W. Wu and V. S. Y. Lin, *Adv. Drug Delivery Rev.*, 2008, **60**, 1278.
- 12 A. Samanta, B. B. Dhar and R. N. Devi, *J. Phys. Chem. C*, 2012, **116**, 1748.
- 13 A. Kumar, V. L. Pushparaj, S. Murugesan, G. Viswanathan, R. Nalamasu, R. J. Linhardt, O. Nalamasu and P. M. Ajayan, *Langmuir*, 2006, **22**, 8631.
- 14 F. Jiao and H. Frei, *Angew. Chem., Int. Ed.*, 2009, **48**, 1841.
- 15 Y. Tian, J. Qi, W. Zhang, Q. Cai and X. Jiang, *ACS Appl. Mater. Interfaces*, 2014, **6**, 12038.
- 16 Z. Li, J. C. Barnes, A. Bosoy, J. F. Stoddart and J. I. Zink, *Chem. Soc. Rev.*, 2012, **41**, 2590.
- 17 I. I. Slowing, B. G. Trewyn, S. Giri and V. S. Y. Lin, *Adv. Funct. Mater.*, 2007, **17**, 1225.
- 18 E. Oliveira, D. Genovese, R. Juris, N. Zaccheroni, J. L. Capelo, M. M. M. Raposo, S. P. G. Costa, L. Prodi and C. Lodeiro, *Inorg. Chem.*, 2011, **50**, 8834.
- 19 W. E. Smith, *Chem. Soc. Rev.*, 2008, **37**, 1042.
- 20 T. M. Cotton, S. G. Schultz and R. P. Vanduyne, *J. Am. Chem. Soc.*, 1980, **102**, 7960.
- 21 D. L. Jeanmaire and R. P. Van Duyne, *J. Electroanal. Chem.*, 1977, **84**, 1–20.
- 22 D. Y. Wu, J. F. Li, B. Ren and Z. Q. Tian, *Chem. Soc. Rev.*, 2008, **37**, 1025.
- 23 L. Rodriguez-Lorenzo, R. A. Alvarez-Puebla, I. Pastoriza-Santos, S. Mazzucco, O. Stephan, M. Kociak, L. M. Liz-Marzahn and F. J. Garcia de Abajo, *J. Am. Chem. Soc.*, 2009, **131**, 4616.
- 24 L. D. Qin, S. L. Zou, C. Xue, A. Atkinson, G. C. Schatz and C. A. Mirkin, *Proc. Natl. Acad. Sci. U. S. A.*, 2006, **103**, 13300.
- 25 J.-J. Feng, U. Gernert, P. Hildebrandt and I. M. Weidinger, *Adv. Funct. Mater.*, 2010, **20**, 1954.
- 26 M. Mahmoudi and V. Serpooshan, *ACS Nano*, 2012, **6**, 2656.
- 27 C.-O. L. Crites, G. L. H. Tapley, M. Frenette, M. G. Béjar, J. C. N. Ferreira and J. C. Scaiano, *ACS Catal.*, 2013, **3**, 2062.
- 28 S. Agnihotri, S. Mukherji and S. Mukherji, *Nanoscale*, 2013, **5**, 7328.
- 29 P. Zhang, C. Shao, Z. Zhang, M. Zhang, J. Mu, Z. Guo and Y. Liu, *Nanoscale*, 2011, **3**, 3357.
- 30 X.-H. Liu, Y.-Y. Cao, H.-Y. Peng, H.-S. Qian, X.-Z. Yang and H.-B. Zhang, *CrystEngComm*, 2014, **16**, 2365.
- 31 J. D. Padmos, M. Langman, K. M. Donald, P. Comeau, Z. Yang, M. Filiaggi and P. Zhang, *J. Phys. Chem. C*, 2015, **119**, 7472.
- 32 Y. Lu, G. Yao, K. Suna and Q. Huang, *Phys. Chem. Chem. Phys.*, 2015, **17**, 21149.
- 33 Z. Zhang, C. Liu, J. Bai, C. Wu, Y. Xiao, Y. Li, J. Zheng, R. Yang and W. Tan, *ACS Appl. Mater. Interfaces*, 2015, **7**, 6211.
- 34 W. Chen, J. Zhang and W. Cai, *Scr. Mater.*, 2003, **48**, 1061.
- 35 C. L. Fang, K. Qian, J. Zhu, S. Wang, X. Lv and S. H. Yu, *Nanotechnology*, 2008, **19**, 125601.
- 36 P. Rameshkumar, S. Saranya, K. Sujathab and R. Ramara, *RSC Adv.*, 2015, **5**, 5038.
- 37 X.-H. Pham, M. Lee, S. Shim, S. Jeong, H.-M. Kim, E. Hahm, S. H. Lee, Y.-S. Lee, D. H. Jeong and B.-H. Jun, *RSC Adv.*, 2017, **7**, 7015.
- 38 Y. Wu, D. Su and D. Qin, *ChemNanoMat*, 2017, **3**, 245.
- 39 M. M. Unterlass, *Eur. J. Inorg. Chem.*, 2016, **8**, 1135.
- 40 F. Lu, D. Sun, J. Huang, M. Du, F. Yang, H. Chen, Y. Hong and Q. Li, *ACS Sustainable Chem. Eng.*, 2014, **2**, 1212.
- 41 J. Virkutyte and R. S. Varma, *Chem. Sci.*, 2011, **2**, 837.
- 42 S. Iravani, *Green Chem.*, 2011, **13**, 2638.
- 43 Y. Hong, X. Jing, J. Huang, D. Sun, T. O. Wubah, F. Yang, M. Du and Q. Li, *ACS Sustainable Chem. Eng.*, 2014, **2**, 1752.
- 44 P. Dauthal and M. Mukhopadhyay, *Ind. Eng. Chem. Res.*, 2016, **55**, 9557.
- 45 S. P. Velammal, T. A. Devi and T. P. Amaladhas, *J. Nanostruct. Chem.*, 2016, **6**, 247.
- 46 J. Kou and R. S. Varma, *ChemSusChem*, 2012, **5**, 2435.
- 47 K. Sapkota and S. S. Han, *New J. Chem.*, 2017, **41**, 5395.
- 48 A. W. Bauer, W. M. Kirby, J. C. Sherris and M. Turck, *Am. J. Clin. Pathol.*, 1966, **45**, 493.
- 49 C. Liu, D. Yang, Y. Jiao, Y. Tian, Y. Wang and Z. Jiang, *ACS Appl. Mater. Interfaces*, 2013, **5**, 3824.
- 50 M. E. El-Tantawy, M. S. Afifi and M. M. Shams, *Can. J. Pure Appl. Sci.*, 2015, **9**, 3365.
- 51 L. Deng, H. Miura, T. Shishido, S. Hosokawa, K. Teramura and T. Tanaka, *Chem. Commun.*, 2017, **53**, 6937.
- 52 S. J. Tauster, S. C. Fung, R. T. K. Baker and J. A. Horsley, *Science*, 1981, **211**, 1121.
- 53 F. W. Lytle, G. H. Via and J. H. Sinfelt, *J. Chem. Phys.*, 1977, **67**, 3831.
- 54 B. Wang, M. Zhang, W. Li, L. Wang, J. Zheng, W. Gan and J. Xu, *Dalton Trans.*, 2015, **44**, 17020.
- 55 S.-K. Li, Y.-X. Yan, J.-L. Wang and S.-H. Yu, *Nanoscale*, 2013, **5**, 12616.
- 56 S. Agnihotri, S. Mukherji and S. Mukherji, *Nanoscale*, 2013, **5**, 7328.
- 57 A. Ahmad, Y. Wei, F. Syed, M. Imran, Z. U. H. Khan, K. Tahir, A. U. Khan, M. Raza, Q. Khana and Q. Yuan, *RSC Adv.*, 2015, **5**, 99364.
- 58 M. Lei, L. Ma and L. Hu, *Tetrahedron Lett.*, 2010, **51**, 4186.
- 59 C. W. Lee, H. Y. Hwang, H. M. Jeong, U. C. Yoon and K.-W. Chi, *Synth. Met.*, 2009, **159**, 1820.
- 60 M. A. Ali, S. M. A. H. Siddiki, W. Onodera, K. Kon and K. Ichi Shimizu, *ChemCatChem*, 2015, **7**, 3555.
- 61 M. Mirza-Aghayan, M. M. Tavana and R. Boukherroub, *Ultrason. Sonochem.*, 2016, **29**, 371.
- 62 P. Kumar, R. K. Pandey, M. S. Bodas, S. P. Dagade, M. K. Dongare and A. V. Ramaswamy, *J. Mol. Catal. A: Chem.*, 2002, **181**, 207.
- 63 R. Luque, V. Budarin, J. H. Clark and D. J. Macquarrie, *Green Chem.*, 2009, **11**, 459.
- 64 I. Mukha, A. Eremenko, G. Korchak and A. Michienkova, *J. Water Resour. Prot.*, 2010, **2**, 131.
- 65 R. Geethalakshmi and D. V. L. Sarada, *Ind. Crops Prod.*, 2013, **51**, 107.
- 66 K. Wang, Y. Wu, H. Li, M. Li, D. Zhang, H. Feng and H. Fan, *RSC Adv.*, 2014, **4**, 5130.



- 67 M. Qasim, B. R. Singh, A. H. Naqvi, P. Paik and D. Das, *Nanotechnology*, 2015, **26**, 285102.
- 68 K. S. Hwan, H.-S. Lee, D.-S. Ryu, S.-J. Choi and D.-S. Lee, *Korean J. Microbiol. Biotechnol.*, 2011, **39**, 77.
- 69 J. C. Stockert, A. Blázquez-Castro, M. Canete, R. W. Horobin and Á. Villanueva, *Acta Histochem.*, 2012, **114**, 785.
- 70 Y. Wu, W. Tang, P. Wang, C. Liu, Y. Yuan and J. Qian, *Part. Part. Syst. Charact.*, 2015, **32**, 779.
- 71 J.-E. Kim, H. Kim, S. S. Aan, E. H. Maeng, M.-K. Kim and Y.-J. Song, *Int. J. Nanomed.*, 2014, **9**, 235.
- 72 X. F. Zhang, W. Shen and S. Gurunathan, *Int. J. Mol. Sci.*, 2016, **17**, 1603.
- 73 P. Wang, X. Wang, L. Wang, X. Hou, W. Liu and C. Chen, *Sci. Technol. Adv. Mater.*, 2015, **16**, 034610.
- 74 M. Priebe, J. Widmer, N. S. Löwa, S.-L. Abram, I. Mottas, A.-K. Woischnig, P. S. Brunetto, N. Khanna, C. Bourquin and K. M. Fromm, *Nanomedicine*, 2017, **13**, 11.

